DEUTSCHES ELEKTRONEN-SYNCHROTRON
INSTITUT FÜR HOCHENERGIEPHYSIK

DESY 93-183
December 1993

The Reaction $e^+e^- \longrightarrow \nu\bar{\nu}b\bar{b}$ and the Higgs Signal at LEP200 and NLC

E. Boos

Nuclear Physics Institute, Moscow State University, Russia

M. Sachwitz, H. J. Schreiber

Deutsches Elektronen-Synchrotron DESY
Institut für Hochenergiephysik IfH, Zeuthen

S. Shichanin

Institute for High Energy Physics, Protvino, Moscow Region, Russia

ISSN 0418-9833

PLATANENALLEE 6 - 15738 ZEUTHEN

To be sure that your preprints are promptly included in the
HIGH ENERGY PHYSICS INDEX,
send them to (if possible by air mail):

DESY **Bibliothek** **Notkestraße 85** **22603 Hamburg** **Germany**	**DESY-IfH** **Bibliothek** **Platanenallee 6** **15738 Zeuthen** **Germany**

DESY 93-183
December 1993

ISSN 0418-9833

The Reaction $e^+e^- \longrightarrow \nu\bar{\nu}\,b\bar{b}$ and the Higgs Signal at LEP200 and NLC

E. Boos[1]
Nuclear Physics Institute, Moscow State University, 119899, Moscow, Russia

M. Sachwitz, H. J. Schreiber
DESY Institute für Hochenergiephysik, Zeuthen, FRG

S. Shichanin[1]
Institute for High Energy Physics, 142284, Protvino, Moscow Region, Russia

[1]Supported by a grant from the Ministry of Science, Research and Culture of the State of Brandenburg

Abstract

A complete tree-level calculation of the reaction $e^+e^- \longrightarrow \nu\bar{\nu}\,b\bar{b}$ in the electroweak standard theory for the energy range of LEP200 and the Next Linear Collider is presented. The matrix elements were calculated by means of the package CompHEP, and phase space integration and event generation were carried out with the computer programs BASES/SPRING. Cross sections for the $\nu\bar{\nu}\,b\bar{b}$ final state, the rate for Higgs production and for different background contributions are studied as a function of the cms energy and the Higgs mass in the range from 80 to 140 GeV. At LEP200 energies, the Higgs bremsstrahlung reaction and the 2-body process $e^+e^- \longrightarrow ZZ$ are dominant while near 500 GeV the Higgs fusion and 2-to-3 body background processes govern the $\nu\bar{\nu}\,b\bar{b}$ final state. Interference patterns were searched for and found to be negligible except for $\sqrt{s} < M_H + M_Z$ where interferences are found to be of comparable strength with the Higgs signal diagrams. Some cancellations between different background diagrams are observed which are expected within the Standard Model. Missing transverse momentum and visible energy distributions for the $\nu\bar{\nu}\,b\bar{b}$ final state indicate some further possibilities to remove background for Higgs searches. A suggestion for an approximate treatment of the reaction $e^+e^- \longrightarrow \nu\bar{\nu}\,b\bar{b}$ is presented so that much computer time can be saved in Monte Carlo simulations.

1 Introduction

The search for the mechanism of the spontaneous symmetry breaking in the Standard Model (SM)[1], in particular for the scalar particle Higgs boson, which appears as a result of the symmetry breaking, is perhaps one of the most fundamental tasks of present high energy physics. Studies for Higgs searches and detailed investigations of the SM Higgs sector have been presented in many publications and are understood quite well (see e.g. ref.'s [2, 3, 4, 5]). The present situation for Higgs searches can be summarized as follows:

- a Higgs boson with $M_H < 65$ GeV could be found at LEP100. The present limit is $M_H \simeq 62.5$ GeV [6];
- the mass interval 65 GeV $\leq M_H \leq$ 100 GeV will be covered by LEP200, including the region $M_H \simeq M_Z$ [7]. The most important reaction for Higgs production is expected to be the bremsstrahlung process

$$e^+e^- \longrightarrow Z^* \longrightarrow H^0 Z \qquad (1)$$

with the H^0 decaying dominantly into the heaviest quark-antiquark system kinematically possible:

$$H^0 \longrightarrow b\bar{b}. \tag{2}$$

There is also the possibility to detect a Higgs particle within this mass interval at the TEVATRON collider in the process $p\bar{p} \longrightarrow W^{\pm}H^0 + X$, $H^0 \longrightarrow b\bar{b}$ [8]. However, this requires increasing the integrated luminosity to about 500 pb^{-1} and invoking a b-jet tagging system of high efficiency;

- the best place to search for an intermediate mass Higgs within the range $M_Z \lesssim M_H \lesssim 2M_Z$ and to study its properties, will be the Next e^+e^- Linear Collider[2] with the center-of-mass (cms) energy of 300 to 500 GeV [9, 10]. In this energy range the fusion mechanism of Higgs production

$$e^+e^- \longrightarrow \nu\bar{\nu}H^0 \tag{3}$$

becomes important due to its cross section rising logarithmically with $\sqrt{s}$. The dominant decay modes of the Higgs boson are $H^0 \longrightarrow b\bar{b}$ for $M_H \lesssim 140$ GeV and $H^0 \longrightarrow WW^*$ for $M_H > 140$ GeV.

An intermediate mass Higgs would also be produced at the future hadron collider LHC [11] in the gluon-gluon fusion process and can be discovered either by the decay $H^0 \rightarrow ZZ^* \rightarrow \mu^+\mu^-\mu^+\mu^-$ where one of the Z is off-shell, or in the rare decay mode $H^0 \rightarrow 2\gamma$. Unfortunately, the event rate after cuts for background reduction is expected to be rather small and, in addition, for the $\gamma\gamma$ decay mode very precise measurements of the photon energies and their directions are required;

- a heavy Higgs (with $M_H \gtrsim 2M_Z$) may be easily discovered at LHC, either in the gold-plated decay mode $H \rightarrow 2Z \rightarrow \mu^+\mu^-\mu^+\mu^-$ or in the silver-plated decay mode $H \rightarrow 2Z \rightarrow \mu^+\mu^-$ 2 jets [12].

Because of the uncritical background conditions expected at future high energy e^+e^- colliders, detailed studies of the SM Higgs sector, namely probing of the couplings of the Higgs and of its spin-parity properties, will remain a domain of the Next Linear Collider (and hopefully already of LEP200).

In a recent paper[14] the 4-fermion final state reaction

$$e^+e^- \longrightarrow \mu^+\mu^- b\bar{b} \tag{4}$$

[2]Next Linear Collider is used as generic name for all e^+e^- linear collider designs presently under study.

has been calculated, with the same technique, as used in this paper, taking into account all tree-level diagrams and their interferences. It has been found that the production and decay characteristics of the H^0 in the bremsstrahlung reaction (1), with the decays $Z \rightarrow \mu^+\mu^-$ and $H^0 \longrightarrow b\bar{b}$, are not affected in a significant way by any possible interference and background terms. Similar results were obtained in ref.[10].

In the present paper a thorough study of the reaction

$$e^+e^- \longrightarrow \nu\bar{\nu}b\bar{b} \tag{5}$$

is reported which might be of interest for several reasons:

- in the case of electron-neutrinos in the final state, Higgs production occurs via two different mechanisms, the bremsstrahlung and the fusion processes, leading to identical 4-fermion final states so that interferences may occur;
- the cross section for Higgs production by fusion rises logarithmically with the cms energy and exceeds the bremsstrahlung contribution at $\sqrt{s} \gtrsim 400$ GeV. Hence, at very large energies (and large Higgs masses) Higgs studies rely mainly on the fusion reaction (3);
- due to the decay of the Z boson into three species of neutrinos and its two times larger branching ratio into each neutrino type as compared to $Z \rightarrow \mu^+\mu^-$, about 6 times more events are expected for the reaction $e^+e^- \rightarrow Z^* \rightarrow ZH^0 \rightarrow \nu\bar{\nu}\,b\bar{b}$ than for the $\mu^+\mu^-\,b\bar{b}$ final state. Thus, channel (5) may allow a more detailed study of the Higgs, in particular at LEP200;
- the large variety of background processes leading to the $\nu\bar{\nu}\,b\bar{b}$ final state, necessitates to obtain precise information on their influence on the apparent production and decay characteristics of the Higgs boson;
- SM properties like gauge invariance and unitarity might be directly investigated because several cancellations between different types of background diagrams are expected to occur;
- since the complete calculation of all contributing diagrams is a large task on any computer, it is desirable to find a simple approximation which can describe the $\nu\bar{\nu}\,b\bar{b}$ final state with high accuracy.

Our calculation for the 4-fermion final state reaction $e^+e^- \longrightarrow \nu\bar{\nu}\,b\bar{b}$ includes all possible tree-level diagrams and their mutual interferences. In particular, Higgs production in the bremsstrahlung and fusion reactions (1) and

(3), with the decays $H^0 \longrightarrow b\bar{b}$ and $Z \longrightarrow \nu\bar{\nu}$, will be discussed in detail. Reaction (3) has already been investigated previously, however, emphasizing the H^0 decays to $WW/ZZ \longrightarrow$ 4-jets, different background diagrams had been taken into account [9]. Also very recently a complete calculation of the reaction $e^+e^- \longrightarrow \nu_e\bar{\nu}_e\, b\bar{b}$ has been done [16]. Since only the subchannel with final state electron-neutrinos was considered, our investigation is more general and adequate for any event number estimation at a given luminosity.

This paper is organized as follows. In sect.2 we present the results of the complete tree-level calculations for the total cross sections of the reaction $e^+e^- \longrightarrow \nu\bar{\nu}\, b\bar{b}$ as well as for the different types of neutrinos in the final state. In sect.3 Higgs production will be investigated. In particular, H^0 cross sections are presented as functions of the energy and the Higgs mass. In sect.4 the contributions of different types of background diagrams are presented, while in sect.5 some particular event distributions for the $\nu\bar{\nu}\, b\bar{b}$ final state are discussed which were recently proposed in order to remove background events. Sect.6 contains our suggestion for an approximate description of the reaction $e^+e^- \longrightarrow \nu\bar{\nu}\, b\bar{b}$ at energies up to about 500 GeV. The summary and concluding remarks are presented in sect.7.

2 The cross section of the reaction $e^+e^- \longrightarrow \nu\bar{\nu}\, b\bar{b}$

The calculation of the process (5), $e^+e^- \longrightarrow \nu\bar{\nu}\, b\bar{b}$, has been performed in the following manner. The generation of Feynman diagrams, the analytical expression for the matrix elements squared and the corresponding optimized FORTRAN codes have been obtained from the computer package CompHEP [17]. The integration over phase space, after smoothing of variables in order to improve the efficiency of the program, and the event generation have been done by employing the Monte Carlo integrator and event generation system BASES/SPRING [18]. The event flow obtained has been incorporated into the program package PYTHIA [19] as an additional process so that all services of this program can be used in the following.

The Feynman diagrams contributing to the process (5) are presented in Fig. 1. The diagrams in the first row correspond to the Higgs signal reactions (1) and (3), with the decays $H^0 \longrightarrow b\bar{b}$ and $Z \longrightarrow \nu\bar{\nu}$. In the case of the electron-neutrino reaction

$$e^+e^- \longrightarrow \nu_e\bar{\nu}_e\, b\bar{b} \tag{6}$$

there exist two signal diagrams, the bremsstrahlung and fusion mechanisms, while in the case of ν_μ/ν_τ production

$$e^+e^- \longrightarrow (\nu_\mu\bar{\nu}_\mu + \nu_\tau\bar{\nu}_\tau)b\bar{b} \tag{7}$$

only the bremsstrahlung mechanism generates the H^0. The second row in Fig.1 involves the ZZ background diagrams which are expected to dominate at LEP200 energies [14]. The third row in this figure corresponds to virtual $Z\gamma^*$ production with subsequent $Z \longrightarrow \nu\bar{\nu}$ and $\gamma^* \longrightarrow b\bar{b}$ decays, while the fourth and fifth rows represent Z and γ^* production via W^+W^- fusion and the single W t-channel exchange diagrams, respectively. Since these diagrams involve charged current exchanges they do not occur in reaction (7). The next two rows in Fig.1 involve the s-channel background diagrams, whereas the last row contains t-channel quark exchange diagrams, which contribute only to ν_e production.

The calculation of the diagrams discussed has been done by assigning non-zero masses to all quarks and Breit-Wigner distributions for the Higgs and Z/W bosons in the intermediate states. In particular, the top quark mass is assumed to be 150 GeV. The SM parameters and the tree-level Higgs width are taken into account. All calculations were carried out in the t'Hooft-Feynman gauge.

Fig.2a shows the cross section for reaction (5), $e^+e^- \longrightarrow \nu\bar{\nu}\, b\bar{b}$, as a function of the cms energy $\sqrt{s}$ at different values of the Higgs mass. In general, after a fast rise the cross sections first decrease with increasing $\sqrt{s}$, and rise at large energies. If $M_H \gtrsim 120$ GeV, an indication for a two-bump structure appears around 220 GeV which is due to the onset of the dominant 2-to-2 body reactions $e^+e^- \longrightarrow ZZ$ and $e^+e^- \longrightarrow H^0Z$ at different thresholds. This observation is supported by Fig.2b where the cross sections for the hypothetical reaction $e^+e^- \longrightarrow (\nu_\mu\bar{\nu}_\mu + \nu_\tau\bar{\nu}_\tau)\, b\bar{b}$ are presented as a function of the cms energy, for the same values of the Higgs mass. Here, H^0 fusion as well as a large part of background diagrams do not contribute. After the fast rise a $1/s$ fall-off follows when the energy is growing, and a two-bump structure appears at low energies if the Higgs mass exceeds the Z mass by more than $\sim$ 20 GeV. The cross section behaviour of this reaction resembles very closely that of reaction (4), $e^+e^- \longrightarrow \mu^+\mu^-\, b\bar{b}$, since the subchannels $e^+e^- \longrightarrow ZZ$ and $e^+e^- \longrightarrow H^0Z$ dominate these 4-fermion final states [14]. The only apparent difference is the larger production rate in the neutrino case due to the two times larger branching ratio of the Z into $\nu\bar{\nu}$ than into $\mu^+\mu^-$, and the summation over two neutrino species in reaction (7). The importance of H^0 fusion and single and double W t-channel exchange diagrams is demonstrated in Fig.2c where $\sigma(e^+e^- \longrightarrow \nu_e\bar{\nu}_e\, b\bar{b})$ is presented as a function of $\sqrt{s}$, for the same five values of the Higgs mass. Here, after the expected threshold behaviour (due to the ZZ

and HZ production channels) the cross section rises with energy for all Higgs masses. A comparison of Figs.2b and 2c reveals that at e.g. $\sqrt{s}$= 500 GeV, the fusion and the W-exchange diagrams dominate the reaction $e^+e^- \longrightarrow \nu\bar{\nu}\,b\bar{b}$.

Values of the cross section for the reaction $e^+e^- \longrightarrow \nu\bar{\nu}\,b\bar{b}$ at different energies and Higgs masses are summarised in Table 1. Assuming an integrated luminosity of 500 pb^{-1} for LEP200 and 10 fb^{-1} for NLC, we expect about 100 events at $\sqrt{s}$ = 200 GeV and M_H = 80 GeV, while about 1500 events would be obtained at 500 GeV for a Higgs mass of 140 GeV. Fig.2a as well as Table 1 shows in addition that in the whole range of LEP200 energies the total cross section for reaction (5) is about a factor of two or more larger if Higgs production is kinematically allowed, as compared with the case of no Higgs production. Therefore, a measurement of the event rate for the process $e^+e^- \longrightarrow \nu\bar{\nu}\,b\bar{b}$ will already provide non-trivial information about the existence of the Higgs boson.

3 The Higgs boson cross section

In this section the contribution of the Higgs boson to the 4-body final state reaction $e^+e^- \longrightarrow \nu\bar{\nu}\,b\bar{b}$ is considered in more detail. As seen in Fig.1, there exist two different mechanisms to produce the Higgs boson. In the bremsstrahlung mechanism, $e^+e^- \longrightarrow H^0Z$ with the subsequent decay of the Z to $\nu_e\bar{\nu}_e$, $\nu_\mu\bar{\nu}_\mu$ or $\nu_\tau\bar{\nu}_\tau$, all neutrino species contribute to the final state, while in the fusion reaction $e^+e^- \longrightarrow \nu\,\bar{\nu}\,H^0$ only electron-neutrinos are produced. Hence, interference between these two mechanisms occurs only for the ν_e component of the reactions.

Fig.3a shows the total Higgs production cross section as a function of $\sqrt{s}$ for Higgs masses between 80 and 140 GeV. In general, after a bump or shoulder at LEP200 energies which is more pronounced the smaller the Higgs mass is, the cross section rises with the increasing $\sqrt{s}$. The individual contributions, namely the bremsstrahlung, the fusion and the interference components, are shown in Figs.3b-d. It can be seen that the low energy bump is entirely due to the bremsstrahlung mechanism. Its strength is less pronounced at large Higgs masses. The rise of the cross section in Fig.3a is caused by the fusion process, $e^+e^- \longrightarrow \nu\,\bar{\nu}\,H^0$, while the interference contribution is small or negligible.

We would like to point out that below the threshold for the bremsstrahlung process, $\sqrt{s_{th}} = M_Z + M_H$, the three possible Higgs production components are rather small and comparable with each other in magnitude. Table 2 collects examples for the bremsstrahlung, fusion and interference cross sections at energies $\sqrt{s} < \sqrt{s_{th}}$. Bremsstrahlung contributions turn out to be non-zero due to the large tail of the Z boson; they however disappear quickly when the distance to the threshold becomes larger. The fusion reaction cross sections (with the threshold at $\sqrt{s} = M_H$) amount to a few fb and do not vary strongly with the cms energy. Interferences in this particular energy region are of about the same strength as the Higgs signal.

Assuming an integrated luminosity of L=500 pb^{-1} for LEP200, the total H^0 event rates expected in the $\nu\bar{\nu}\,b\bar{b}$ final state at energies $\sqrt{s} < \sqrt{s_{th}}$ are presented in Table 3. We would like to emphasize that in order to get the correct number of such events at energies below or very close to $\sqrt{s_{th}}$ the bremsstrahlung, fusion and interference contributions all have to be taken into account.

In Figs.4a-d the total Higgs cross section as well as the individual contributions are presented as a function of M_H for three energies $\sqrt{s}$ = 200, 300 and 500 GeV. At LEP200 energies, σ is dominated by the bremsstrahlung contribution as long as the Higgs mass is smaller than $\sim$ 110 GeV (see Fig.4b). The fusion contribution while is dominating at 500 GeV, decreases almost linearly with increasing M_H; the dependence on M_H is however less pronounced at smaller cms energies. Interference terms are close to zero and do not depend strongly on the Higgs mass.

4 The background diagrams

In this section the contributions corresponding to the Feynman diagrams in rows 2-7 of Fig.1 are discussed. In order to obtain a deeper understanding of their behaviour it is also worthwile to study the contributions separately for the $\nu_e\bar{\nu}_e\,b\bar{b}$ and $(\nu_\mu\bar{\nu}_\mu + \nu_\tau\bar{\nu}_\tau)\,b\bar{b}$ final states. Fig.5 presents the total background rate as well as the background rates for the electron and μ/τ neutrino channels as a function of $\sqrt{s}$. The general behaviour of the overall cross section resembles very closely the cross section behaviour of reaction (5), $e^+e^- \longrightarrow \nu\bar{\nu}\,b\bar{b}$, which includes the Higgs contributions (see Fig.2). At LEP200 energies the ν_μ/ν_τ background is dominant while background terms leading to ν_e's become more important with increasing energy. If one adds to the results for the total background of Fig.5 those of the Higgs production seen in Fig.3a, cross section values are obtained which are very close to those of the overall reaction $e^+e^- \longrightarrow \nu\bar{\nu}\,b\bar{b}$, which are presented in Fig.2a. Thus, interferences between these components are very small. More details of the background behaviour can be obtained from Fig.6 where for three different types of background terms and for their coherent sum, the ν_e cross sections are

shown as a function of $\sqrt{s}$. The ZZ and $Z\gamma^*$ background rates are large at LEP200 energies but less important at the NLC. In contrast, the Z/γ (row 4 in Fig.1) and single Wt-channel exchange cross section (row 5 in Fig.1) increase with growing energy, exceeding their coherent sum significantly at $\sqrt{s} \gtrsim 300$ GeV. We are faced here with special cancellations between different diagrams due to the gauge invariance and unitarity properties of the SM. They would not occur in this way for non-standard model vertex structures, e.g. if anomalous magnetic moments for the W and Z bosons would exist. The experimental confirmation of these cancellations would therefore provide further support to the SM.

The remaining background diagrams in Fig.1, namely the s-channel contributions (rows 6 and 7), are negligible because of the additional suppression factor of the order of the electroweak coupling α_W. This is in accord with the results for reaction (4) in ref. [14]. The cross sections for these contributions are about 0.1-0.2 fb at cms energies between 180 and 500 GeV.

The last row of diagrams in Fig.1 consists of diagrams with quark exchange in the t-channel. We expect that the rates for c- and u-quark exchange are negligible due to the very small values of the corresponding Kobajashi-Maskawa angles. The cross sections from the diagram with top quark exchange turn out to be also very small: it is $\sim$ 0.1 fb at $\sqrt{s}$ =300 GeV and $\sim$0.2 fb at $\sqrt{s}$ =500 GeV. Variations of the top quark mass between 120 and 190 GeV produce only unimportant changes in the cross section of reaction (5). For instance, at $\sqrt{s}$ = 500 GeV the $\nu\bar{\nu}\,b\bar{b}$ cross section amounts to 149 fb for M_{top} = 120 GeV and to 146 fb for M_{top} = 190 GeV.

5 More details about the $\nu\bar{\nu}\,b\bar{b}$ events

In this section detailed properties of reaction (5), $e^+e^- \longrightarrow \nu\bar{\nu}\,b\bar{b}$, will be discussed. In particular, differential distributions are presented which have been discussed in e.g. ref.'s [7, 13] as being useful to discriminate against various QCD and W^+W^- background processes while retaining the H^0 signal from the fusion reaction.

Fig.7 shows the number of events expected at $\sqrt{s}$ = 200 GeV and M_H= 80 GeV assuming a luminosity of 500 pb^{-1}, as a function of the $b\bar{b}$ invariant mass, the visible energy and the missing transverse momentum. In the $b\bar{b}$ invariant mass distribution (Fig.7a) clear peaks from the H^0 and Z bosons appear, whereas background contributions are completely negligible. The visible energy (defined as the sum of the b- and $\bar{b}$-quark energies) is shown in Fig.7b for all $\nu\bar{\nu}\,b\bar{b}$ events and for the H^0 events (hatched histogram), which were

selected by requiring M($b\bar{b}$) close to the H^0 mass. The unrestricted spectrum indicates a two spike behaviour; the first corresponds to the bremsstrahlung process $e^+e^- \longrightarrow H^0 Z$, with the energy of the Higgs boson, $E_H \simeq (s + M_H^2 - M_Z^2) \,/\, 2\sqrt{s}$, close to 95.2 GeV. The position of the second spike comes from the dominating background reaction $e^+e^- \longrightarrow ZZ$, with $E_Z \simeq \sqrt{s}\,/2 =$ 100 GeV.

Fig.7c presents the missing $p_\perp$-distribution which is calculated as the sum of the b- and $\bar{b}$-quark transvers momenta. The hatched histogram contains only the H^0 events. Possible structures in this spectrum correspond to the largest missing $p_\perp$-momenta of the Z boson in the two reactions $e^+e^- \longrightarrow ZZ$ and H^0Z, with $p_\perp^{max} = \sqrt{s - M_Z^2} = 41.0$ GeV and $p_\perp^{max} = \{[s - (M_Z + M_H)^2][s - (M_Z - M_H)^2]\}^{1/2}/2\sqrt{s} = 51.6$ GeV, respectively.

As a second example, we present the analogous distributions at $\sqrt{s}$ = 500 GeV and M_H = 140 GeV in Figs.8a-c. The number of events entering these plots are normalized to an integrated luminosity of 10 fb^{-1}. Clear peaks from the Z and H^0 bosons are visible in the $b\bar{b}$ invariant mass distribution, which allows again a simple H^0 selection by a cut around M_H. The visible energy distribution (Fig.8b) reveals some interesting structures. A part of them is caused by the H^0 events (hatched spectrum): it involves a broad bump around 160 GeV, with a gentle fall-off with increasing E_{vis} and possesses a one-bin narrow spike close to 260 GeV. This spike is due to the bremsstrahlung reaction $e^+e^- \longrightarrow H^0 Z$ resulting to a fixed H^0 energy of $(s + M_H^2 - M_Z^2)/2\sqrt{s} = 261$ GeV. The broad bump is associated with the fusion reaction $e^+e^- \longrightarrow \nu\bar{\nu}H^0$, which starts at $E_{vis} = M_H$. The remaining narrow spike in Fig.8b is caused by the 2-body reaction $e^+e^- \longrightarrow ZZ$ with $E_{vis} \simeq \sqrt{s}\,/2 = 250$ GeV, and the structure around 100 GeV is due to the fusion channel $e^+e^- \longrightarrow \nu\bar{\nu}Z^0\,/\gamma^*$. Fig.8c shows the missing $p_\perp$-distribution, again for all $\nu\bar{\nu}\,b\bar{b}$ events as well as for the Higgs events (hatched histograms). Both distributions are similar, so that this variable is not very helpful to select H^0 events from background in the $\nu\bar{\nu}\,b\bar{b}$ final state at $\sqrt{s}$ = 500 GeV.

6 The approximation scheme

The calculation of the complete set of diagrams for the reaction $e^+e^- \longrightarrow \nu\bar{\nu}\,b\bar{b}$ is rather CPU-time and memory consuming. It is therefore worthwhile to search for a rapid and effective approximation for detailed Monte Carlo simulations of the $\nu\bar{\nu}\,b\bar{b}$ final state. It has been demonstrated in [14] that the reaction $e^+e^- \longrightarrow \mu^+\mu^-\,b\bar{b}$ can be well approximated by an incoherent sum of the Higgs bremsstrahlung process, $e^+e^- \longrightarrow H^0 Z$, and the most important

2-to-2 background channels, $e^+e^- \longrightarrow ZZ \,/\, Z\gamma^*$, with the subsequent decays $Z/\gamma^* \longrightarrow \mu^+\mu^-$ and $H^0/Z \longrightarrow b\bar{b}$. The situation for reaction (5) however is more complicated, because the strength of the different terms varies considerably with cms energy. This is demonstrated in more detail in Fig.9 where the difference of the cross sections for the complete calculation and the approximated 2-to-2 calculation (in analogy to ref.[14]), with subsequent H^0, Z and γ^* decays, is shown as the function of the energy (dashed curve). While at LEP200 energies reasonable agreement is found, with increasing $\sqrt{s}$ the difference rises to reach $\sim$ 25% at 500 GeV indicating the importance of diagrams so far neglected, as e.g. the H^0 and Z/γ^* fusion and single W t-channel exchange. By adding these diagrams, corresponding to the 2-to-3 body reactions $e^+e^- \longrightarrow \nu\bar{\nu}H^0/Z/\gamma^*$, incoherently to the 2-to-2 body scheme mentioned above, the cross section difference (solid line in Fig.9) now decreases to well below 3% in the whole range $\sqrt{s} = 180$ GeV to 500 GeV. Possible Higgs mass dependences are canceled in this quantity. The gain in computer time achieved with this approximation, as compared to the full calculation, is about a factor of 15.

7 Summary and conclusions

In this paper the 4-body final state reaction $e^+e^- \longrightarrow \nu\bar{\nu}\,b\bar{b}$ has been studied at LEP200 and NLC energies. Calculations of the cross section within the Standard Model were carried out either with the complete tree-level set of diagrams or with different subsets of them, in order to gain an understanding of the importance of the individual contributions.

For a Higgs boson with a mass in the range between 80 and 140 GeV, two mechanims are relevant for its production. The bremsstrahlung mechanism which produces all neutrino species in the final state, dominates at LEP200 energies while the fusion mechanism which allows only ν_e production, is most important at $\sqrt{s} = 500$ GeV. Interferences between the two mechanisms are found to be very small. They are however of a strength comparable with the total production cross section at energies just below the threshold of the bremsstrahlung process, $M_H + M_Z$. Whether under such circumstances a Higgs signal can be seen remains open since the event rate is small (for an optimistic LEP200 integrated luminosity of 500 pb^{-1}, 5 to 15 events are expected to be produced). Differential distributions, like visible energy or missing transvers momentum distributions of the $\nu\bar{\nu}\,b\bar{b}$ final state which have been suggested to remove a large part of the QCD and W^+W^- background events, indeed present some possibilities to further reduce the $\nu\bar{\nu}\,b\bar{b}$ background while retaining the

H^0 signal.

From an investigation of the relative importance of the different diagrams contributing to the reaction $e^+e^- \longrightarrow \nu\bar{\nu}\,b\bar{b}$ (shown in Fig.1) the following conclusions are drawn:

- at LEP200 energies, most of the cross section is due to the bremsstrahlung Higgs mechanism $e^+e^- \longrightarrow H^0 Z$ and the 2-to-2 body background reactions $e^+e^- \longrightarrow ZZ/Z\gamma^*$, with subsequent $H^0 \longrightarrow b\bar{b}$ and $Z/\gamma^* \longrightarrow \nu\bar{\nu}$ or $b\bar{b}$ decays;
- around $\sqrt{s} = 500$ GeV, the fusion process dominates H^0 production, and the background fusion reactions $e^+e^- \longrightarrow \nu\,\bar{\nu}\,Z^0\,/\gamma^*$ as well as the single W t-channel exchange reactions are becoming important;
- the quark exchange diagrams, in particular that with top quark exchange, are negligible ($\sim$ 0.1% of the total cross section) at all energies studied;
- the s-channel background contributions (corresponding to the diagrams in rows 6 and 7 of Fig.1) are negligible as well ($\sim$ 0.1-0.2%);
- interferences between the diagrams are very small;
- cancellations between fusion and single W t-channel exchange diagrams are found; i.e. the individual cross sections are larger than the coherent sum at $\sqrt{s} \gtrsim 300$ GeV. These cancellations are an intrinsic property of the Standard Model;
- the incoherent sum of the processes $e^+e^- \longrightarrow H^0 Z$, $e^+e^- \longrightarrow \nu\,\bar{\nu}\,H^0$, $e^+e^- \longrightarrow ZZ\,/Z\gamma^*$ and $e^+e^- \longrightarrow \nu\,\bar{\nu}\,Z^0\,/\gamma^*$, with the subsequent $H^0 \longrightarrow b\bar{b}$ and $Z/\gamma^* \longrightarrow \nu\bar{\nu}$ or $b\bar{b}$ decays, describes the complete cross section of the reaction $e^+e^- \longrightarrow \nu\bar{\nu}\,b\bar{b}$ with high accuracy, i.e. the deviations from the full calculation are $\lesssim$ 2% between $\sqrt{s} = 180$ GeV and 500 GeV, for Higgs masses of 80 GeV to 140 GeV. Hence, such an approximation is useful for detailed $\nu\bar{\nu}\,b\bar{b}$ Monte Carlo studies.

Acknowledgements

We would like to thank P. Zerwas for many valuable discusions concerning our results. We are grateful to V. Ilyin and A.Pukhov for the help in using the latest CompHEP version. E.B. thanks M. Dubinin for providing preliminary results of a similar investigation for the reaction $e^+e^- \longrightarrow \nu_e\bar{\nu}_e\,b\bar{b}$. E. B. and S. Sh. would like to thank P. Soeding for his interest and support as well as DESY-IfH Zeuthen and the Zeuthen L3 group for the kind hospitality.

References

[1] S. L. Glashow, Nucl. Phys. **22** (1961) 579;
S. Weinberg, Phys. Rev. Lett. **19** (1967) 1264;
A. Salam, Elementary Particle Theory, ed. by N. Svartholm, Stockholm (1968), 367.

[2] H. E. Haber, in Physics and Experiments with Linear Colliders, ed. by R. Orava, P. Eerola and M. Nordberg, World Scientific Publishing Co.,1992, p. 235.

[3] J. F. Gunion, H. E. Haber, G. Kane and S. Dawson, The Higgs Hunter's Guide, Addison-Wesley 1990;

[4] A. Djouadi, D. Haidt and P. M. Zerwas, Proc. of the Workshop - Munich, Annecy, Hamburg, 1991, ed. by P. M. Zerwas, DESY Report 92-123A, p. 1;
A Djouadi, D. Haidt, B. A. Kniehl, B. Mele and P. M. Zerwas, Proc. of the Workshop - Munich, Annecy, Hamburg, 1991, ed. by P. M. Zerwas, DESY Report 92-123A, p. 11.

[5] P. Janot, LAL preprint 93-38 (July 1993), talk given at the Second Int. Workshop on Physics and Experiments with Linear e^+e^- Collider, Waikoloa, Hawaii, 1993.

[6] G. Coignet, talk given at the XVI Int. Symposium on Lepton-Photon Interactions Ithaca, New York, August 1993.

[7] S. L. Wu et al., Proc. of the ECFA workshop, Aachen 1988, ed. by A. Böhm and W. Hoogland, CERN Report 87-08, p. 312;
R. Kleiss, Z. Kunszt and W. J. Stirling, Phys. Lett. **B242** (1990) 507;
N. Brown, Z. Phys. **C49** (1991) 657.

[8] E. Boos et al., D0 note 1719/93 (unpublished), FNAL, 1993.

[9] V. Barger, K. Cheung, B. A. Kniehl and R. Phillips, Phys. Rev. **D46,** (1992) 3752.

[10] V. Barger, K. Cheung, A. Djouadi, B. A. Kniehl and P. M. Zerwas, DESY prepeprint 93-064 (June 1993), subm. to Phys. Rev. D.

[11] A. Rubbia, talk given at the Second Int. Workshop on Physics and Experiments with Linear e^+e^- Collider, Waikoloa, Hawaii, 1993.

[12] J. F. Gunion and G. L. Kane, Proc. of the 1990 summer Study on High Energy Physics, 1990, Snowmass, Colorado, p. 59.

[13] P. Grosse-Wiesmann, D. Haidt and H. J. Schreiber, Proc. of the Workshop - Munich, Annecy, Hamburg, 1991, ed. by P. M. Zerwas, DESY Report 92-123A, p. 37.

[14] E. Boos, M. Sachwitz, H. J. Schreiber and S. Shichanin, DESY preprint 93-089 (July 1993), subm. to Z. f. Phys.

[15] S.Komamiya, in Physics and Experiments with Linear Colliders, ed. by R. Orava, P. Eerola and M. Nordberg, World Scientific Publishing Co., 1992, p. 277.

[16] M. Dubinin, V. Edneral, Y. Kurihara and Y. Shimizu, private communication.

[17] E. E. Boos et al., Proc. of the XXVIth Recontre de Moriond, ed. by J. Tran Than Van, Edition Frontiers, 1991, p. 501;
E. E. Boos et al., Proc. of the Second Int. Workshop on Software Engineering, ed. by D. Perred-Gallix, World Scientific, 1992, p. 665;
E. E. Boos et al., KEK preprint 92-47, 1992.

[18] S. Kawabata, Comp. Phys. Commun. **41** (1986) 127.

[19] T. Sjöstrand, PYTHIA5.6 and JETSET7.3, preprint CERN-TH. 6488/92.

Table Caption

Tab. 1: Cross sections (in fb) for the reaction $e^+e^- \longrightarrow \nu\bar{\nu}\,b\bar{b}$ for different cms energies and Higgs boson masses.

Tab. 2: Cross sections (in fb) for Higgs boson production in the $\nu\bar{\nu}\,b\bar{b}$ final state at energies $\sqrt{s} < M_H + M_Z$.

Tab. 3: Number of Higgs boson events expected in the $\nu\bar{\nu}\,b\bar{b}$ final state at energies $\sqrt{s} < M_H + M_Z$ for a luminosity of 500 pb^{-1}.

Figure Caption

Fig. 1: Feynman diagrams contributing to the reaction $e^+e^- \longrightarrow \nu\bar{\nu}\,b\bar{b}$.

Fig. 2: Cross sections as functions of the cms energy for
a) the reaction $e^+e^- \longrightarrow \nu\bar{\nu}\,b\bar{b}$,
b) the reaction $e^+e^- \longrightarrow (\nu_\mu\bar{\nu}_\mu + \nu_\tau\bar{\nu}_\tau)\,b\bar{b}$ and
c) the reaction $e^+e^- \longrightarrow \nu_e\bar{\nu}_e\,b\bar{b}$,
for five Higgs masses in the range of 80 to 140 GeV.

Fig. 3: H^0 cross sections as functions of the cms energy for
a) the reaction $e^+e^- \longrightarrow \nu\bar{\nu}\,b\bar{b}$,
b) the reaction $e^+e^- \longrightarrow (\nu_\mu\bar{\nu}_\mu + \nu_\tau\bar{\nu}_\tau)\,b\bar{b}$,
c) the reaction $e^+e^- \longrightarrow \nu_e\bar{\nu}_e\,b\bar{b}$ and
d) the interference contribution,
for five Higgs masses in the range of 80 to 140 GeV.

Fig. 4: H^0 cross sections as functions of the Higgs mass for the reaction $e^+e^- \longrightarrow \nu\bar{\nu}\,b\bar{b}$ at $\sqrt{s} = 200$, 300 and 500 GeV.
In Figs. 4b to 4c the full curve corresponds to the fusion mechanism, the dotted curve to the bremstrahlung mechanism and the dashed curve to the interference pattern.

Fig. 5: Background cross sections for the reaction $e^+e^- \longrightarrow \nu\bar{\nu}\,b\bar{b}$ as functions of the cms energy.

Fig. 6: Different background cross sections contributing to the reaction $e^+e^- \longrightarrow \nu_e\bar{\nu}_e\,b\bar{b}$ as a function of the cms energy.

Fig. 7: Number of events expected for $L = 500$ pb^{-1} in
a) the $b\bar{b}$ invariant mass distribution,
b) the visible energy distribution and
c) the missing transverse momentum distribution
at $\sqrt{s} = 200$ GeV and a Higgs mass of 80 GeV.
The hatched distributions correspond to the H^0 events.

Fig. 8: Number of events expected for L = 10 fb^{-1} in
a) the $b\bar{b}$ invariant mass distribution,
b) the visible energy distribution and

c) the missing transverse momentum distribution
at $\sqrt{s} = 500$ GeV and a Higgs mass of 140 GeV.
The hatched distribution corresponds to the H^0 events.

Fig. 9: Difference of the complete $\nu\bar{\nu}\,b\,\bar{b}$ cross section
and the 2-to-2 body approximation (dashed curve)
as well as the proposed approximation of the incoherent sum of the 2-to-2
and 2-to-3 body reactions (full curve).

$\sqrt{s}, GeV$	M_H, GeV				
	80	M_Z	100	120	140
160	15	9.3	7.3	5.4	5.2
170	37	13	9.8	6.9	6.3
180	145	31	20	15	14
190	205	152	79	63	61
200	217	185	153	82	79
300	150	141	135	121	109
500	194	186	179	161	148

Table 1:

	Bremsstrahlung	Fusion	Interference
$M_H = 80$ $\sqrt{s} = 165$	6.6	3.9	3.8
$M_H = 80$ $\sqrt{s} = 170$	20.4	4.6	5.6
$M_H = 91.2$ $\sqrt{s} = 170$	9.3	4.0	4.0
$M_H = 100$ $\sqrt{s} = 190$	9.3	3.8	3.8
$M_H = 110$ $\sqrt{s} = 200$	7.8	3.5	3.1

Table 2:

	$M_H = 80$ $\sqrt{s} = 165$	$M_H = 80$ $\sqrt{s} = 170$	$M_H = 91.2$ $\sqrt{s} = 180$	$M_H = 100$ $\sqrt{s} = 190$	$M_H = 110$ $\sqrt{s} = 200$
N_{events}	7	15	9	8	7

Table 3:

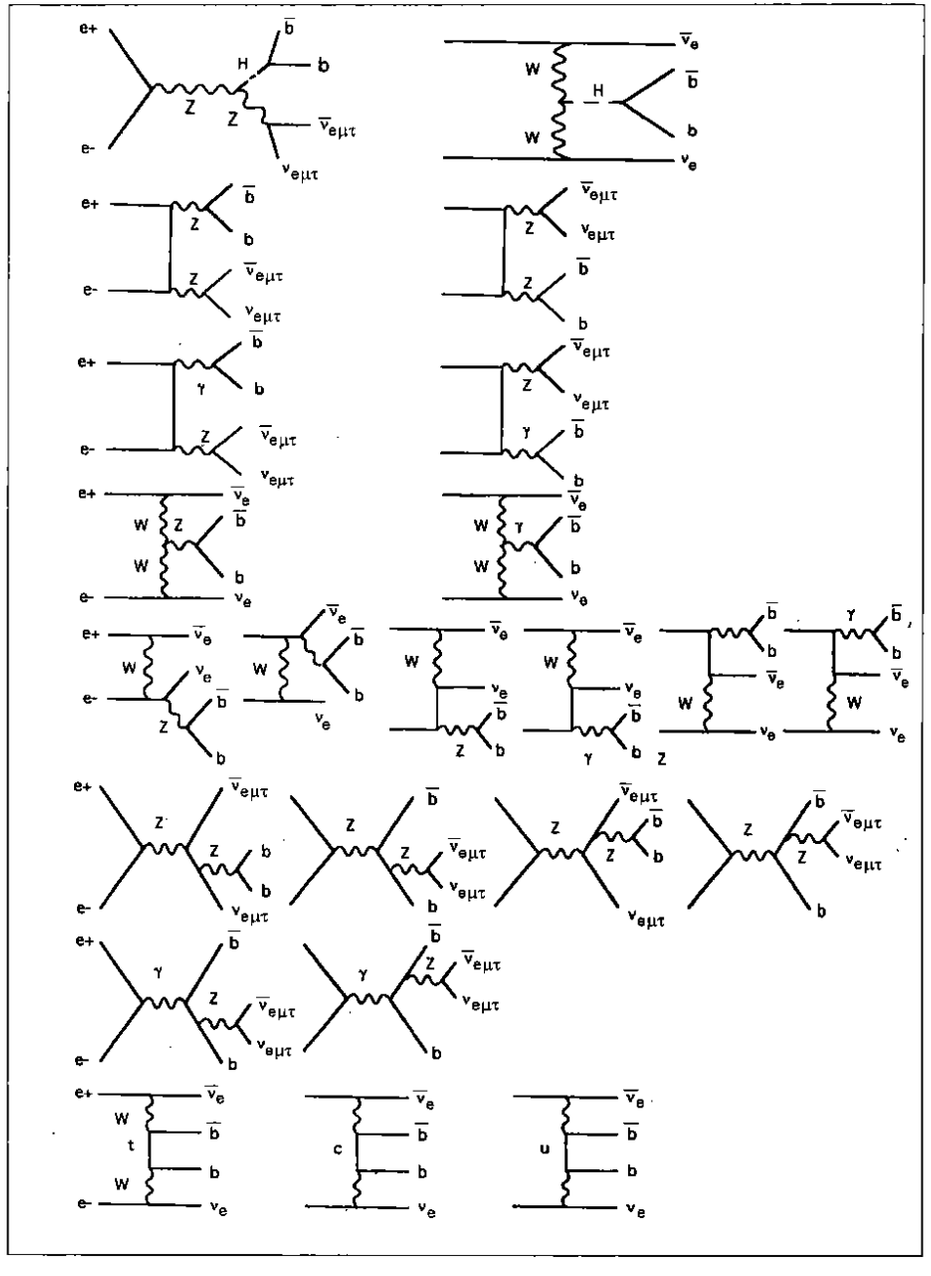

Figure 1:

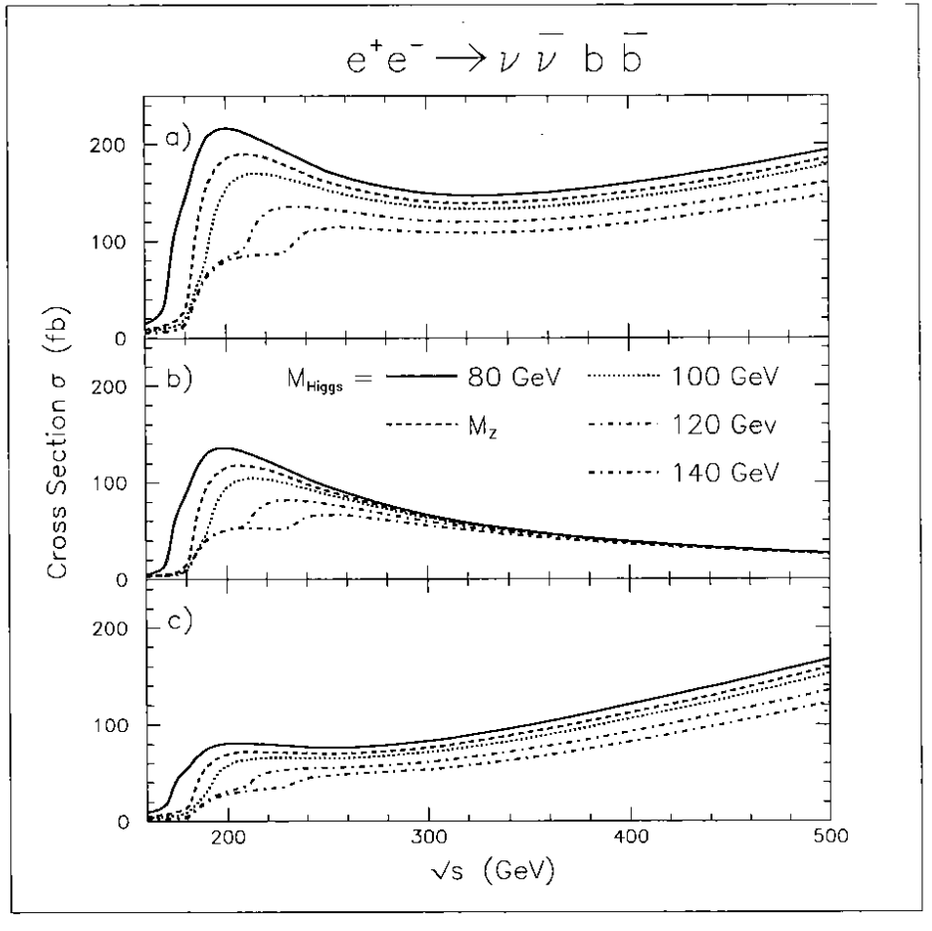

Figure 2:

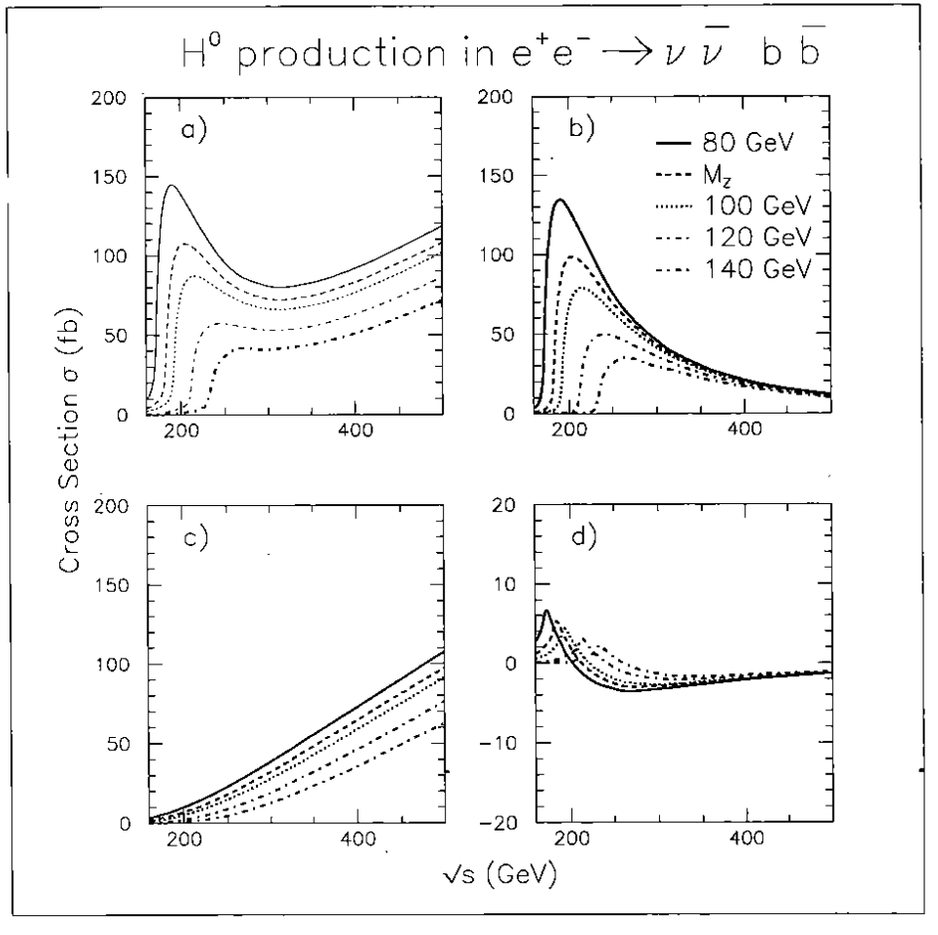

Figure 3:

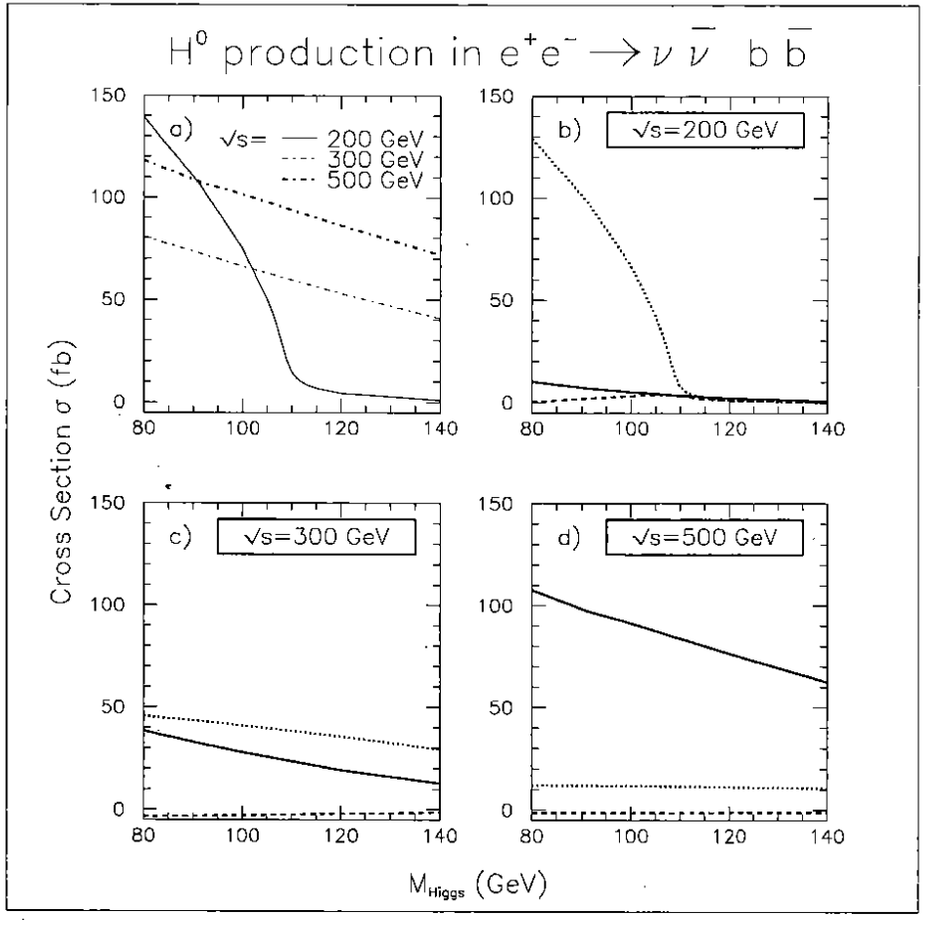

Figure 4:

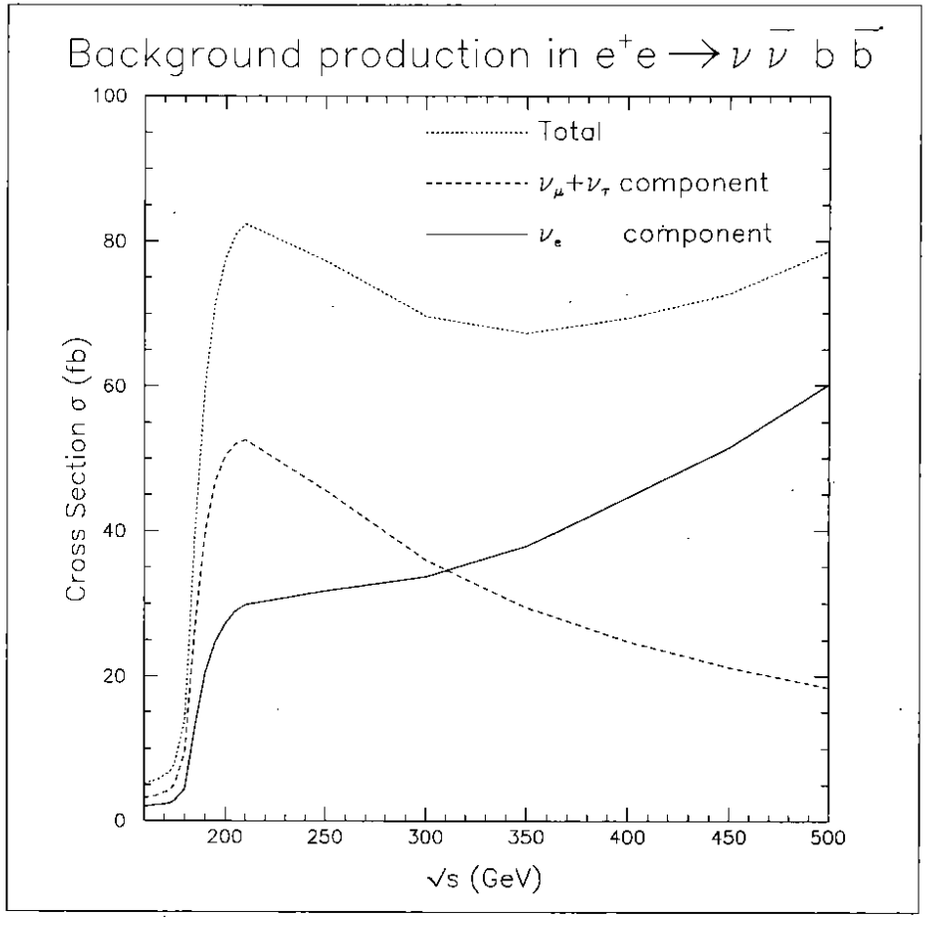

Figure 5:

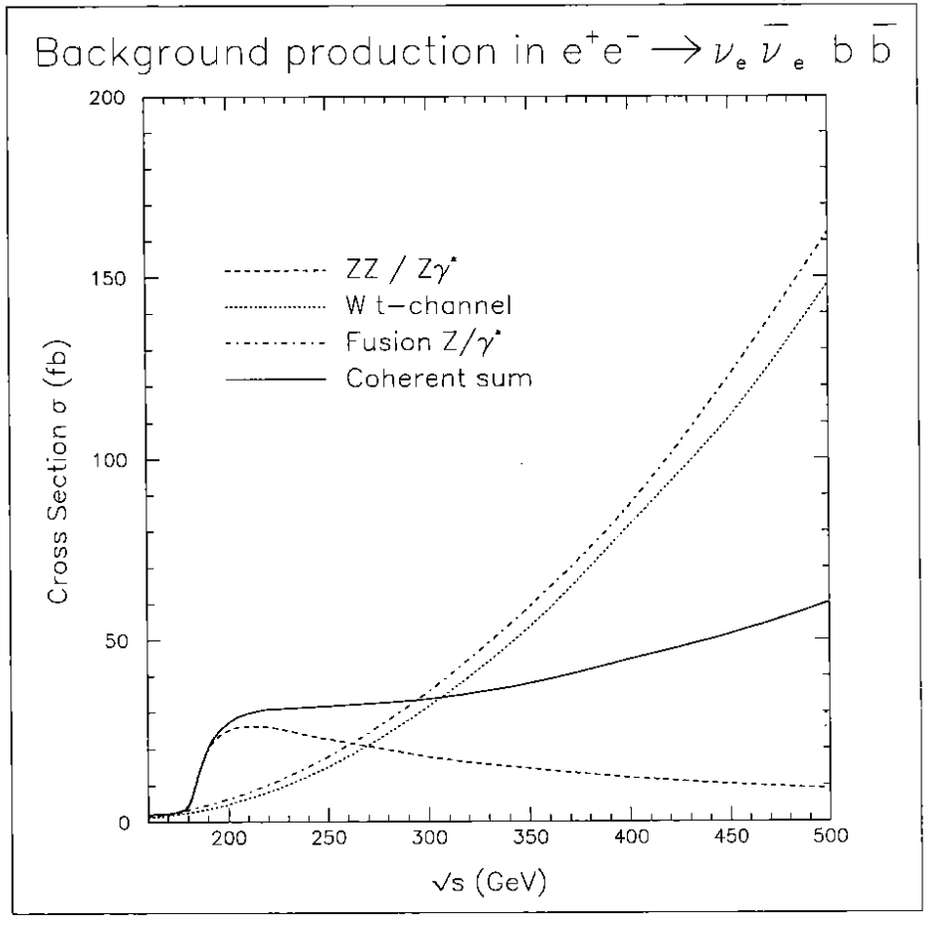

Figure 6:

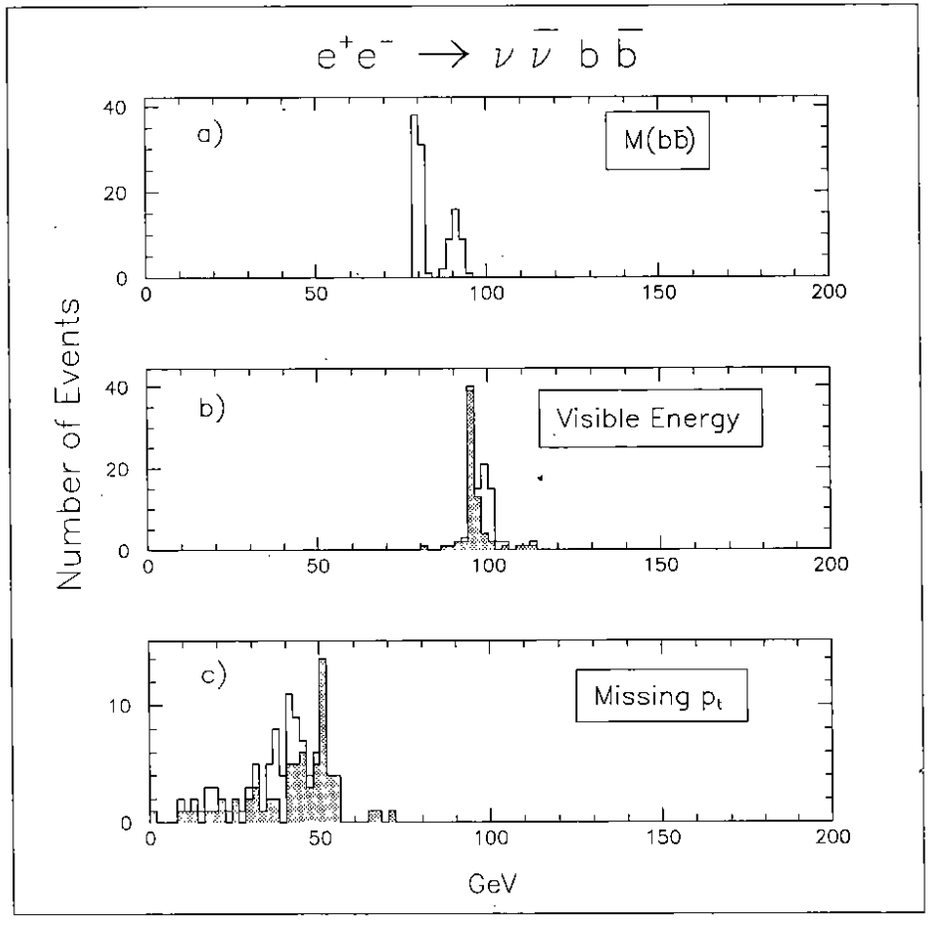

Figure 7:

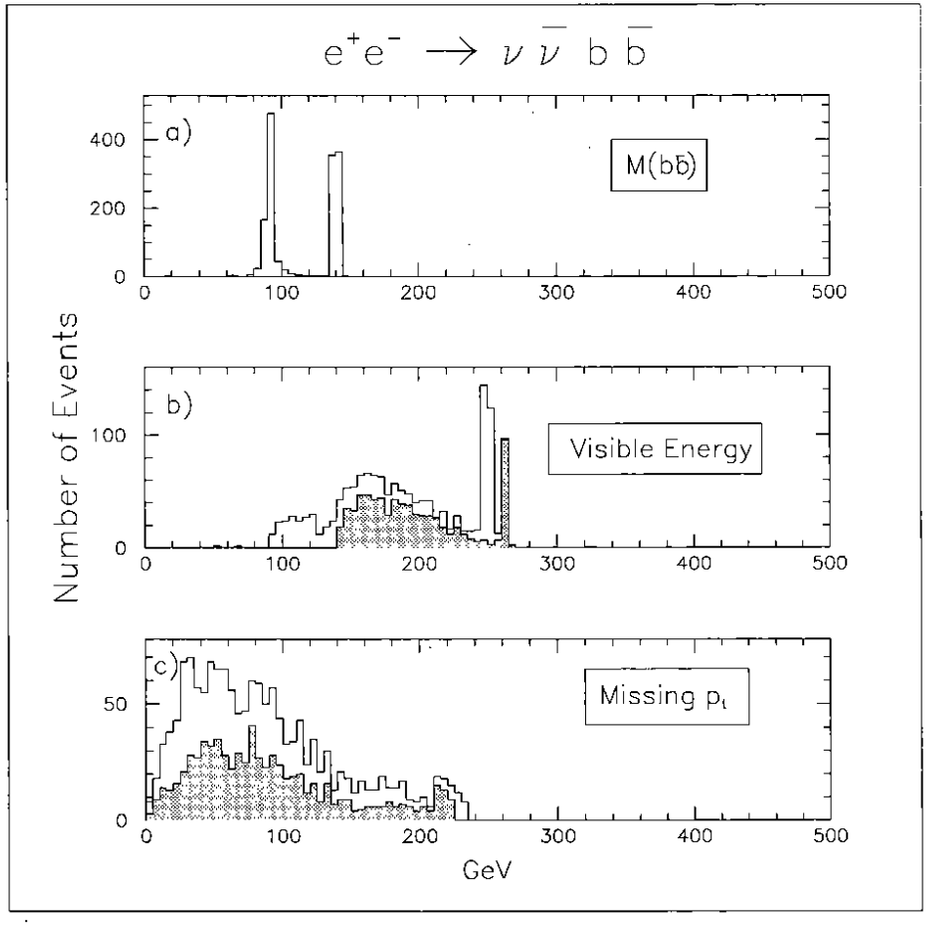

Figure 8:

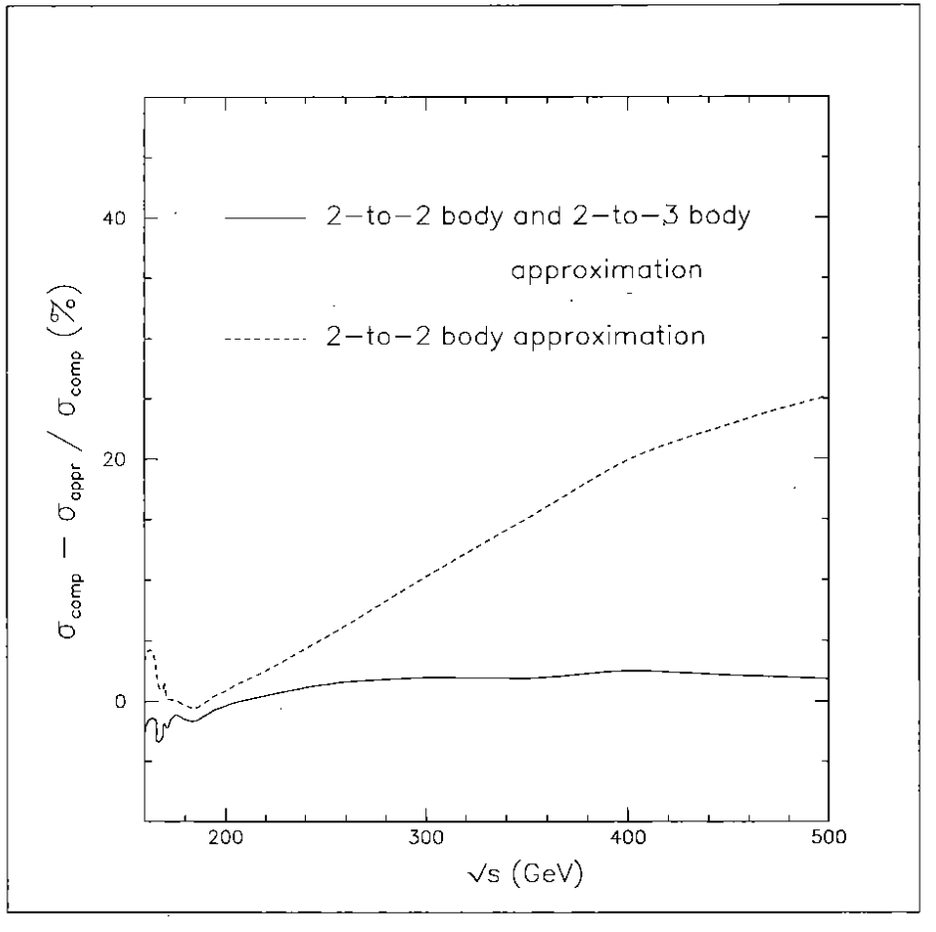

Figure 9: